Bonham, J. A., Faers, M. A., & van Duijneveldt, J. S. (2018). Binary and ternary mixtures of microgel particles, hard spheres and non-adsorbing polymer in non-aqueous solvents. *Colloids and Surfaces A. Physicochemical and Engineering Aspects*, *536*, 180-190. https://doi.org/10.1016/j.colsurfa.2017.07.022

Colloids and Surfaces A xxx (xxxx) xxx–xxx

Contents lists available at ScienceDirect

Colloids and Surfaces A

journal homepage: www.elsevier.com/locate/colsurfa

Binary and ternary mixtures of microgel particles, hard spheres and non-adsorbing polymer in non-aqueous solvents

J.A. Bonham[a,*], Malcolm A. Faers[b], Jeroen S. van Duijneveldt[a,*]

[a] School of Chemistry, University of Bristol, Cantock's Close, Bristol BS8 1TS, UK
[b] Bayer AG, Crop Science Division, Alfred-Nobel-Str. 50, D-40789 Monheim, Germany

GRAPHICAL ABSTRACT

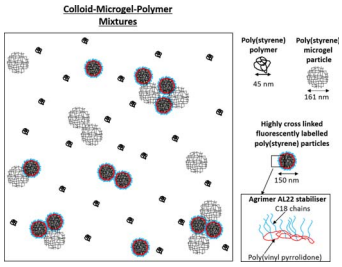

ARTICLE INFO

Keywords:
Colloid
Polymer
Microgel
Depletion interaction
Hard spheres

ABSTRACT

Crosslinked polystyrene (PS) particles were dispersed in diisopropyl adipate, a non-volatile, good solvent for PS. Depletion attractions between particles were induced by adding linear PS, with a polymer/particle size ratio of 0.3. For hard particles, with a high crosslink density, the colloid–polymer mixtures displayed phase separation in agreement with predictions for hard sphere–polymer mixtures. For similar sized but weakly crosslinked, soft microgel particles however, a significantly higher concentration of linear PS needed to be added to observe phase separation. This is because the non-adsorbing polymer can penetrate the soft microgels which weakens the depletion interaction.

In ternary mixtures of the hard and soft particles and linear PS, confocal microscopy reveals that mixed particle networks are formed. Upon adding soft particles to a hard particle gel network, there is only modest variation in the flow properties, with the moduli decreasing somewhat, yet viscosity increasing. It is argued that the effect of an increase of volume fraction is offset by a reduction in depletion interaction strength. This demonstrates that, in these ternary mixtures, microgels act like particles rather than polymer depletants; yet microgel addition allows high volume fraction polymer–colloid mixtures to be made whilst avoiding the viscosity increase that would normally result.

1. Introduction

Model systems using hard or nearly hard spheres play a key role in colloidal science experiments; the simplicity of these particles enables theoretical comparisons with experimental data as well as easy access to a multitude of different particle sizes, chemistries and interactions [1]. The study of colloid–polymer mixtures is no exception and a vast proportion of the literature on these systems is on model hard spheres, in particular on poly(methyl methacrylate) particles in cis-decalin with non-adsorbing poly(styrene) [2]. The critical minimum polymer volume fraction, $\phi^{\dagger}$, needed to induce flocculation, depends on a large number of variables, including the size ratio between the polymer and

* Corresponding authors.
E-mail addresses: Jessica.Bonham@bristol.ac.uk (J.A. Bonham), J.S.van-Duijneveldt@bristol.ac.uk (J.S. van Duijneveldt).

http://dx.doi.org/10.1016/j.colsurfa.2017.07.022
Received 31 October 2016; Received in revised form 19 June 2017; Accepted 8 July 2017

the colloid, the polymer molecular weight, the colloid volume fraction and the solvency [3].

Nonetheless, the colloidal particle "hardness" also affects $\phi^{\dagger}$. For soft particles in a theta solvent, the non-adsorbing polymer is able to penetrate the colloid and thus the depletion interaction is weakened. In a good solvent, the effect of the interpenetration is restricted [4]. Furthermore, the polymer will penetrate the soft particle less when the colloidal particles and non-adsorbing polymer are incompatible [5]. For hard particles there is no penetration and thus the samples are less stable to flocculation.

There is very little literature on the use of soft microgel particles in the depletion induced phase separation, and in most studies involving microgel particles they are modelled as hard spheres [6–10]. Weakly cross-linked microgel particles however, are not hard [1] and particle softness is important when determining the phase separation of microgel–polymer mixtures [11]. Saunders and Vincent studied the effect of non-adsorbing polymer on lightly cross-linked microgel particles. Initially, osmotic deswelling of the particles occurred on addition of non-adsorbing polymer and on increasing the polymer concentration further, the deswollen particles flocculated [12]. Clarke and Vincent looked at the depletion of crosslinked microgel particles in ethyl benzene with added poly(styrene). They saw that $\phi^{\dagger}$ depended on the extent of swelling of the microgels which determines whether the particles can be modelled as hard or soft particles [13].

The majority of literature on colloid–polymer mixtures focuses on binary mixtures where the interactions between non-adsorbing polymer and one type of hard colloidal particle are probed. In real industrial systems, however, complex formulations are used where multiple hard and/or soft particles are included in the formulations [14]. It is therefore timely to seek a description going beyond hard sphere mixtures.

The study of ternary mixtures, where two types of colloidal particles are mixed with non-adsorbing polymer, could enhance the understanding of the interactions and phase behaviour of real, industrial formulations. However, the literature on such systems is limited. Schmidt and Denton studied ternary mixtures of colloidal spheres, ideal polymer and thin needles. A rich phase behaviour was observed, where a region of three coexisting phases could be achieved by varying the particle sizes and concentrations. A geometry based density functional theory was applied to the bulk fluid phases and used to predict demixing [14]. Additionally, non-spherical rod and platelet particles were used in ternary mixtures by Esztermann et al. where a geometry based density functional theory was also used [15].

Whilst there is literature on both ternary mixtures and on mixtures with soft particles, there is little literature on the study of mixtures which include both hard and soft colloidal particles. Hennequin et al. studied the phase behaviour of asymmetric colloidal particles where the particle softness was varied using a sterically stabilising layer. They studied three different types of mixtures, where the particle softness of both the large and small particles was varied. However, the phase behaviour of their mixtures was not greatly affected by the particle softness [16]. There is no known literature on the phase behaviour of ternary mixtures that include both hard and soft particles with non-adsorbing polymer. Such a system would provide a better model for industrial formulations which include multiple types of particles.

This work looks at both binary and ternary microgel and/or hard sphere–polymer mixtures. Highly cross-linked, fluorescently labelled poly (styrene) latex particles are used as the hard particles and lightly cross-linked poly(styrene) microgel particles are used as the soft particles. Both types of particles have a hydrodynamic radius of ca. 80 nm so that the effect of particle hardness rather than particle size can be determined.

In particular, we are interested in how the soft microgel particles affect the phase behaviour of the mixtures, which is analysed using differential interference contrast microscopy and macroscopic images, and the strength of any networks that are formed during the depletion interaction which is measured using rheology. Confocal laser scanning microscopy is also used to examine the structures formed.

Table 1
Description of particles used in binary and ternary mixtures. Hydrodynamic radii were determined in water (r_0) and DIA (r_H).

Particle	Description	XLD[a]	r_0/nm	r_H/nm	q_r[b]
Microgel	Poly(styrene) microgel particles	1/80	36	80.5	0.28
Fluorescent poly (styrene)	Fluorescently labelled poly (styrene) latex particles stabilised with AL22	1/10	69	75	0.3
Polymer	Poly(styrene) with M_w = 498,000 g mol^{-1}	–	–	22.5[c]	–

[a] Cross-link density expressed as the molar ratio between monomer and cross-linker.
[b] $q_r = r_G/r_H$.
[c] Radius of gyration r_G.

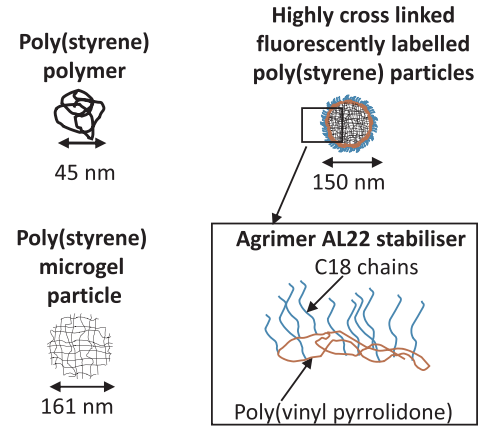

Fig. 1. Schematic diagram of the three types of particles used in the binary and ternary mixtures.

2. Experimental

Three types of particles were used in the binary and ternary mixtures: microgel particles, hard sphere, fluorescently labelled particles and non-adsorbing polymer, see Table 1 and Fig. 1. The following section describes the synthesis of both the microgels and the fluorescently labelled particles, the sample preparation and characterisation. Linear poly(styrene) with a molecular weight, M_w of 498,000 g mol^{-1} and an M_w/M_n<1.2, was purchased from Pressure Chemical Company.

2.1. Materials

Styrene (S), potassium persulfate (KPS), sodium dodecylbenzenesulfonate (SDBS), divinylbenzene (55%) (DVB) and Sudan 2 were purchased from Sigma–Aldrich. Methacryloxyethyl thiocarbamoyl rhodamine B was purchased from Polysciences Europe GmbH. Agrimer AL22 was kindly supplied by Ashland. Prior to the reaction, the styrene was run through a column to remove any inhibitor. Styrene, KPS and DVB were kept at 278 K before use.

The solvent chosen for the binary mixtures was diisopropyl adipate (DIA) which was donated by Croda. This solvent was chosen as it is swells the microgel particles well but also has a low volatility, and thus the solvent will not evaporate during experiments; this was a particular concern for rheological experiments. Whilst DIA is commercially important as a solvent, there is little data regarding this solvent available in the literature.

2.2. Particle synthesis

2.2.1. Microgel particle synthesis

The microgel particles were made via an emulsion polymerisation according to Ref. [17]. The total reaction volume was 400 ml. 90.22 wt % water was mixed with 0.14 wt% SDBS in a 3-necked round bottomed

flask connected to a reflux condenser and exposed to an argon atmosphere. The mixture was stirred at 500 rpm for 10 min. 3.22 wt% styrene and 0.05 wt% DVB were then added and stirred for a further 15 min. 0.12 wt% KPS initiator, dissolved in 3.75 wt% water and washed with another 2.5 wt% water, was then added and the reaction was heated at 338 K for 24 h.

After cooling to room temperature, the product was run through glass wool to remove any partially polymerised residues and then dialysed against deionised water for two weeks, until the conductance was stable. The water was removed using a rotary evaporator and the solid white particles were dried in a vacuum oven overnight.

2.2.1.1. Fluorescent microgel particles. Lightly cross-linked microgel particles were dyed with Sudan 2, a fluorescent dye. Initially 0.252 g of microgel particles were dispersed in 12 ml tetrahydrofuran, THF (99.9%, VWR Chemicals) with 0.022 g Sudan 2. The microgel particles were homogenised by tumbling overnight. THF is a good solvent for poly(styrene), hence the particles were highly swollen and the dye molecules could penetrate into the interior of the particles during dispersion. Any dye that was not taken up by the particles was removed by centrifuging the solutions at 20,100 g for 25 min using a Labnet Prism Microcentrifuge (24 place rotor, 230 V). The supernatant was replaced with fresh THF and the process was repeated three times. The THF was then removed in a rotary evaporator and the particles were dried in a vacuum oven overnight.

2.2.2. Fluorescent poly(styrene) particles

For the hard spheres, highly cross-linked poly(styrene) and divinylbenzene microgel particles were made via an emulsion polymerisation. The cross-link density, expressed as a molar ratio of monomer: cross-linker was 1/10. Methacryloxyethyl thiocarbamoyl rhodamine B, a fluorescent dye with an excitation wavelength of 548 nm and an emission wavelength of 570 nm was incorporated into the particles during the synthesis. During propagation, the terminal vinyl groups at the end of the dye decompose in the presence of free radicals and hence the dye becomes chemically linked to the particles.

An aqueous phase of 92.89 wt% water and 0.025 wt% SDBS was mixed and degassed with argon. An oil phase of 5.59 wt% styrene, 1.41 wt% DVB, 0.08 wt% KPS and 3.5×10^{-3} wt% methacryloxyethyl thiocarbamoyl rhodamine B was prepared separately. The two phases were then combined in a 3-necked round bottomed flask, connected to a reflux condenser and stirred using an overhead mechanical stirrer at 300 rpm. The solution was mixed under an atmosphere of argon for 15 min before the temperature was increased to 363 K. The reaction was carried out for 24 h.

After cooling to room temperature, the product was run through glass wool to remove any partially polymerised residues and then dialysed for two weeks, until the conductance was stable. The water was removed using a rotary evaporator and the solid pink particles were dried in a vacuum oven overnight.

The fluorescent dye changes the surface chemistry of the particles and hence they no longer disperse in diisopropyl adipate without the aid of a stabilising polymer. Agrimer AL22, a commercial comb copolymer with a poly(vinyl pyrrolidone) backbone and 80% C18 side chains, was used to stabilise the fluorescently labelled poly(styrene) particles. A stock solution of fluorescently labelled poly(styrene) particles stabilised with AL22 in DIA was made with a volume fraction of 0.27. For a 10 ml stock solution, 4.2 g particles were initially dispersed in 3 ml DIA and a slurry was formed. The sample was homogenised using a high shear mixer (Silverson L4RT) for 5 min and then placed in a sonic bath (IND 500D, Ultrawave) for a further 5 min. During these steps any aggregates between the particles were broken up. Separately, 2×10^{-4} g AL22 was stirred in 3 ml DIA, which had previously been heated to ca. 323 K to dissolve the polymer. The two solutions were combined and homogenised using the high shear mixer for 5 min and then left stirring overnight. Dynamic light scattering was used to measure the particle size and confirm that the particles were fully dispersed.

2.3. Characterisation

The particles were dispersed in DIA and their hydrodynamic size was determined by dynamic light scattering using a Malvern Autosizer 4800 with a wavelength of 532 nm at 298 K. The microgel particles were dissolved in fresh solvent at a concentration of ca. 5 mg ml^{-1}. For the highly cross-linked, fluorescent poly(styrene) particles the stock solutions were diluted until the particle concentration was ca. 5 mg ml^{-1}. All of the solutions were filtered with a 5 μm Millipore filter to remove any dust particles. Readings were taken multiple times to ensure reproducible results. To analyse the light scattering data, the refractive indices of the solvents were measured using an Abbé refractometer where the temperature was controlled using a water bath.

The radius of gyration of the non-adsorbing poly(styrene) polymer was determined using a Brookhaven multiangle BI-200SM goniometer with a BI-900AT digital signal processor and a wavelength of 488 nm. The angle was varied from 30 to 150°, the pin hole was set to 1 mm and the power was 0.1 W. The dark count average was 579 s^{-1} and 5 repeats were taken for each angle, where the dust rejection multiplier was 3. 0.2 vol.% solutions were prepared and samples were filtered using a 5 μm Millipore filter before use to remove any dust. A ratio of the sample intensity and the intensity of pure toluene was determined; the intensity was also corrected for the scattering intensity of the pure solvent. For pure DIA solvent it was assumed that the solvent exhibited Rayleigh scattering, where the scattering intensity is independent of the scattering angle. R_g of the polymer was determined using a Guinier analysis.

An Olympus BX-51 differential interference contrast (DIC) microscope with a 40× objective was used to observe the mixtures. This technique highlights refractive index gradients in the focal plane and hence is very useful for detecting phase separation of colloidal particles. The samples were homogenised using a vortex mixture prior to imaging. A pipette was used to draw a drop of the sample onto a glass slide and a cover slip was placed on top of the sample. Although DIA is a non-volatile solvent, clear nail polish was used to seal the sample before images were taken.

After microscopic images were taken, the samples were left to stand for at least 3 weeks, and images were taken every week. These images were used to study the height and appearance of the phase separation. Height profiles were obtained from the images by measuring the H/H_0 after 7 days, where H is the height of the bottom layer in the sample and H_0 is the total sample height.

The rheology of the samples was measured using a Malvern Kinexus Pro Rheometer controlled by rSpace software with a 20 mm diameter, 4° cone and plate geometry. Shear rate sweeps were carried out, where the shear rates were varied from 0.01 to 1200 s^{-1} with 11 readings taken per decade. Two sweeps were carried out for each sample where initially the viscosity was measured with increasing shear rate. Once this sweep was finished the viscosity was remeasured with a decreasing shear rate.

Frequency sweeps were also carried out for each sample. The frequency sweep must be measured in the linear viscoelastic region of the sample, that is where the rheological properties are independent of the shear strain [17]. To determine the linear viscoelastic region of the samples, a shear strain sweep between 0.01 and 1% strain was performed and an appropriate shear strain for the frequency sweep was chosen. Two frequency sweeps were then measured, where the frequencies probed ranged from 2 Hz, for a weak sample or 5 Hz, for a stronger sample to 0.001 Hz. An average of the moduli at 0.5 Hz was taken and used to compare different samples. An example of these sweeps is shown in the Supplementary Information.

Confocal laser scanning microscopy, CLSM (Leica SP5 fitted with a resonant scanner) was used to image the fluorescently labelled poly

Table 2
Concentrations and volume fractions of binary and ternary mixtures.

Sample	F conc. (g ml^{-1})	F ϕ	M conc. (g ml^{-1})	M ϕ	Total conc. (g ml^{-1})	Total ϕ
MP0.10	0	0	0.009	0.10	0.009	0.10
MP0.20	0	0	0.018	0.20	0.018	0.20
FP0.13	0.105	0.13	0	0	0.105	0.13
FP0.27	0.21	0.27	0	0	0.210	0.27
MFP0.23	0.105	0.13	0.009	0.10	0.114	0.23
MFP0.37	0.21	0.27	0.009	0.10	0.219	0.37
MFP0.46	0.21	0.27	0.018	0.20	0.228	0.46

M = microgel particles, F = highly cross-linked fluorescent hard spheres, P = non-adsorbing polymer.

(styrene) particles and mixtures. A rectangular glass capillary with inner dimensions of 0.10 mm × 1.00 mm (Vitrocom) was filled with the suspensions and sealed on each end with epoxy glue. For the binary mixtures, the excitation wavelength was 543 nm and a 63 × oil immersion objective was used. For the ternary mixtures where two different fluorescent particles were used, two different excitation channels were also used with a 63 × oil immersion objective. For the rhodamine B hard sphere particles an excitation wavelength of 543 nm was used and for the Sudan 2 microgel particles, an excitation wavelength of 420 nm was used. For qualitative imaging of the gel structure, 2D (512 × 512 pixels), and 3D (full scan of the capillary in the z direction) data sets were recorded.

2.4. Determination of particle volume fractions

Before the sample preparation is described, it is important here to discuss how the volume fractions are calculated and the errors associated with them. The volume fraction of the particles is determined by first calculating the volume fraction of an equivalent unswollen, dense particle. This is done by dividing the mass of the particle per unit of volume by the poly(styrene) density, 1.05 g ml^{-1}. The volume fraction of swollen particles is then larger than that of the unswollen particles by a factor $(r_H/r_0)^3$, where the swollen hydrodynamic radius, r_H, was measured using DLS.

The microgel particles are highly swollen in solvent and hence this is a viable technique to analyse the particle volume fraction. The fluorescently labelled particles, however are highly cross-linked and therefore should not swell significantly in solvent. Nonetheless, the DLS experiments suggest that the particles swell slightly in solvent and hence r_H is also used to calculate ϕ for these particles.

The volume fractions of the hard sphere–microgel mixtures are determined by adding the calculated ϕ values for the two components together. The main drawback of calculating ϕ in this way is that any errors associated with the dynamic light scattering measurements are then incorporated into the particle concentrations.

2.5. Sample preparation

The ratios of concentrations of microgels and hard sphere particles were varied to produce 7 different binary and ternary mixtures, see Table 2. For each mixture, the polymer concentration was also varied.

To prepare the mixtures, initially the individual particles and polymer were dispersed in DIA separately and the two components were then mixed together. The initial particle volume fractions were twice as large as the final volume fractions, as mixing the two components halved each volume fraction.

For microgel–polymer (MP) mixtures, solid microgel particles were dispersed in 1.5 ml DIA in 3.5 ml vials; these vials were homogenised overnight by tumbling on rollers. Two different particle volume fractions were studied, MP0.10 and MP0.20.

A concentrated polymer solution was also prepared in a similar manner to the microgel solutions. The polymer concentrations are expressed in c_p/c^* where c_p is the polymer concentration in g ml^{-1} and c^* is the polymer overlap concentration:

$$c^* = \frac{3M_w}{4\pi R_g^3 N_A}, \tag{1}$$

where M_w is the polymer molecular weight. The radius of gyration, R_g, for the polymer used in these experiments was measured using static light scattering and was 22.5 nm, corresponding to a polymer overlap concentration of 17.5 mg ml^{-1}. The desired polymer concentration was added to the microgel solutions and for some concentrations, additional DIA was needed, to make a total sample volume of 3 ml.

For fluorescent poly(styrene)–polymer (FP) mixtures, the stabilisation of the particles in DIA is described in Section 2.2.2. FP mixtures with a volume fraction of 0.13 were made by adding 0.75 ml of the concentrated particle solution to a 1.75 ml vial, the desired concentration of polymer solution was then added. Ternary microgel–fluorescent particle–polymer (MFP) mixtures with an overall volume fraction of 0.23 were made in the same manner described above.

As the stock solution had a volume fraction of 0.27, it was not possible to dilute this further when making FP0.27 mixtures. Therefore, for these mixtures, solid poly(styrene) was added directly to the stock solution in 1.75 ml vials. For MFP0.37 and MFP0.46, it was also not possible to dilute the stock particle solutions as the initial volume fractions were too high. Therefore, 1.5 ml of stock particle solution was added to either a 1.75 ml or 3 ml vial and solid microgel particles were added. Solid poly(styrene) was also added in the same manner as above. This does, however result in slightly lower volume fractions then previously stated, as the overall volume is slightly higher than 1.5 ml. Consequently MFP0.37 mixtures actually have a microgel volume fraction of 0.099 and a hard sphere volume fraction of 0.268. Additionally, MFP0.46 mixtures have a microgel volume fraction of 0.197 and a hard sphere volume fraction of 0.265. All the above mixtures were homogenised by tumbling for at least 12 h before any characterisation was carried out.

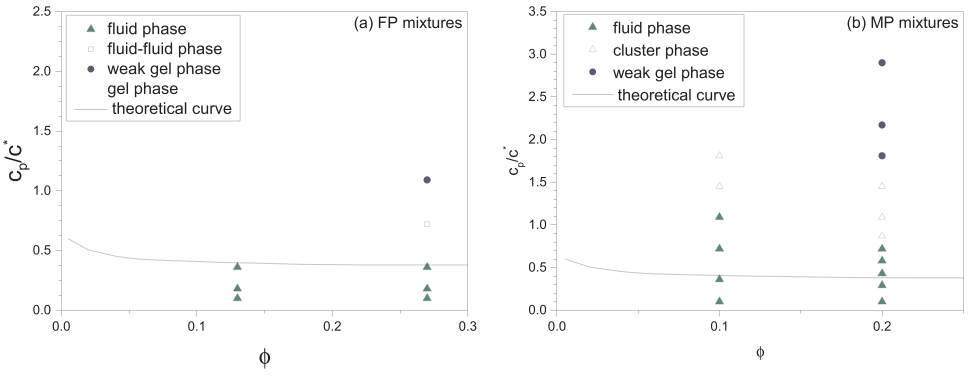

Fig. 2. Phase diagrams of fluorescent poly(styrene)–polymer mixtures (a) and microgel–polymer mixtures (b). Green triangles = stable fluid, red triangles = cluster formation, blue circles = weak gel, black circles = gel and purple square = fluid–fluid separation. The solid line shows the theoretical curve from Ref. [18] where q_r = 0.34. (For interpretation of the references to color in this figure legend, the reader is referred to the web version of the article.)

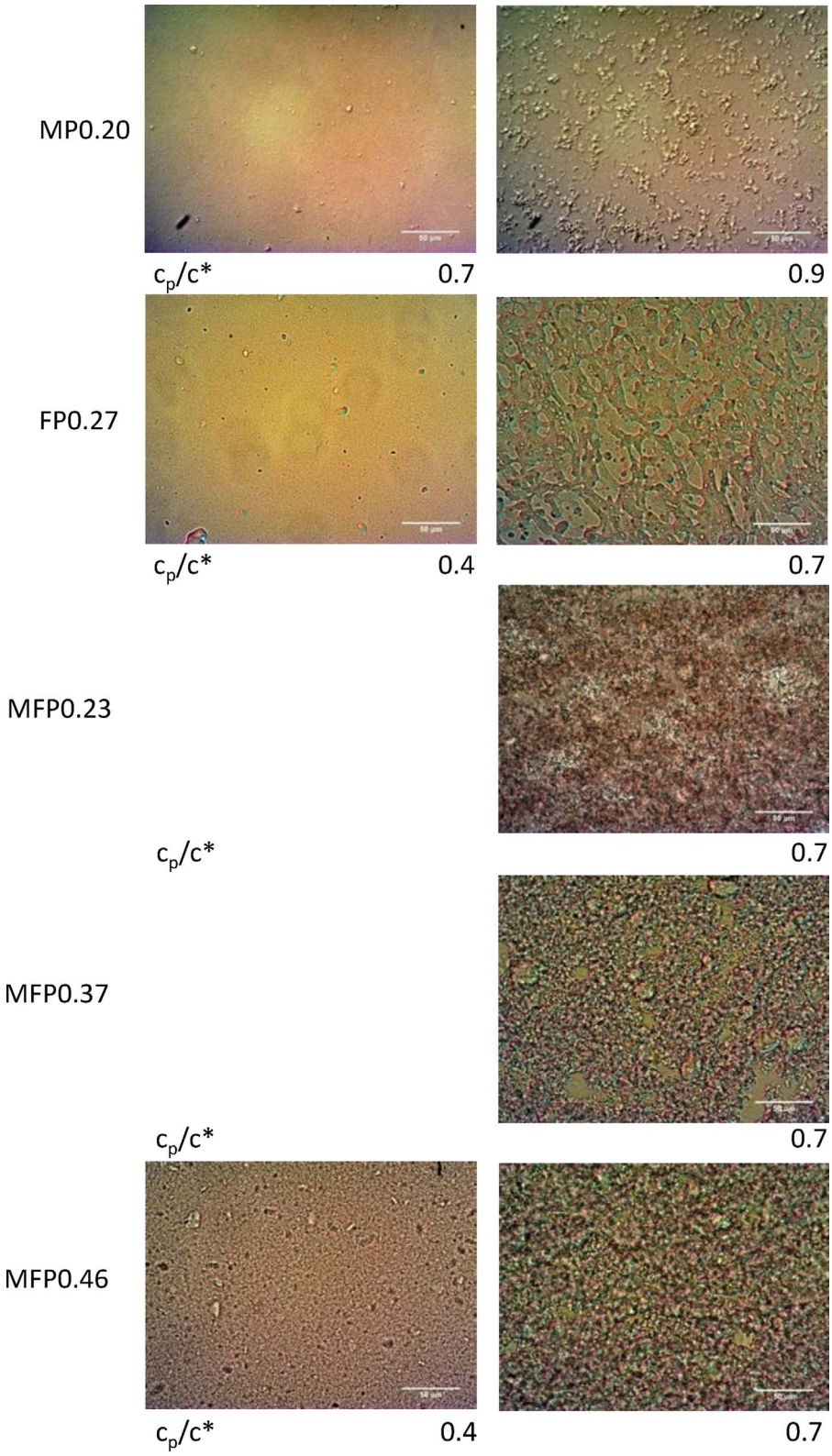

Fig. 3. DIC images of the binary and ternary mixtures. The polymer concentration, in c_p/c^* is indicated below each image. The scale bar in each image is 50 μm.

3. Results

A brief description of each type of particle used in the following binary and ternary mixtures is given in Table 1. The hydrodynamic radius is 75 nm and 80.5 nm for the fluorescent poly(styrene) particles and the microgels respectively corresponding to a size ratio, q_r, of 0.28–0.3.

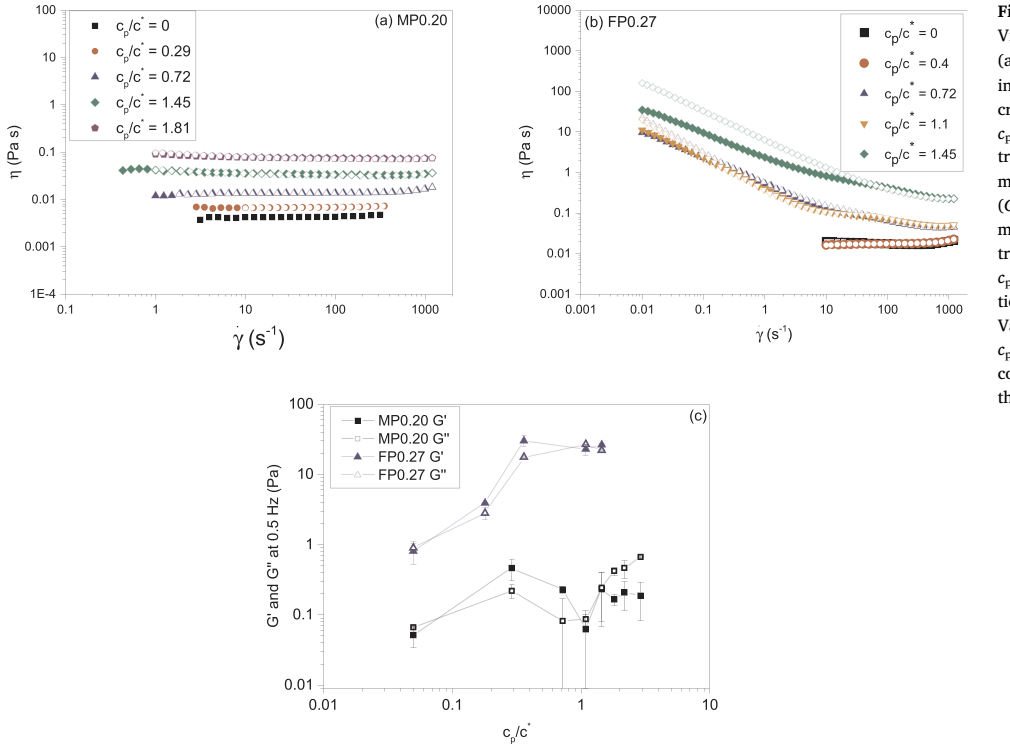

Fig. 4. Rheology of binary mixtures. (a) and (b) Viscosity, η, as a function of shear rate, $\dot{\gamma}$, for MP0.20 (a) and FP0.27 (b) mixtures. Filled symbols are for increasing shear rate and open symbols are for decreasing shear rate. The polymer concentrations in c_p/c^* are 0 (black squares), 0.3 (red circles), 0.7 (blue triangles), 1.1 (orange triangles), 1.45 (green diamonds) and 1.8 (purple pentagons). (c) The elastic (G' – filled symbols) and viscous (G'' – open symbols) moduli of MP0.20 (black squares) and FP0.27 (blue triangles) as a function of polymer concentration in c_p/c^*. G' and G'' were taken from frequency oscillation sweeps at 0.5 Hz. Lines are to guide the eye. Values shown at $c_p/c^* = 0.05$ actually correspond to $c_p/c^* = 0$. (For interpretation of the references to color in this figure legend, the reader is referred to the web version of the article.)

3.1. Binary mixtures

DIC microscopy, height profiles and rheology measurements were all used to gain an overall picture of the phases formed when non-adsorbing poly(styrene) is added to both hard sphere and microgel particles. The experimental results are plotted as a phase diagram and compared to the free volume perturbation theory for a mixture of hard sphere colloids and interacting polymer with a size ratio of 0.34 [18], see Fig. 2. Five different regimes are seen: fluid, cluster phase, fluid–-fluid phase separation, weak gel and strong gel. A sample is described as a weak gel if the DIC microscopy images and height profiles suggest that a network is forming, but the rheological experiments do not provide evidence of a network in the sample. For a sample to be described as gel, rheology, DIC microscopy and the height profiles all indicate that a network has formed in the sample.

For the FP mixtures, the fluid–solid phase boundary agrees well with theoretical predictions from the literature, see Fig. 2a. For FP0.13 mixtures there is no region where a weak gel is formed and the samples transition directly from a fluid to a gel at $c_p/c^* = 0.7$. For FP0.27 mixtures a fluid–fluid phase separation is observed at $c_p/c^* = 0.7$. Although this fluid–fluid separation is not expected, the size ratio used can produce fluid phases on rare occasions and it is expected that this fluid–fluid region of the phase diagram is narrow [7]. For FP0.27 mixtures a weak gel is formed when $c_p/c^* = 1.1$ and gel is formed when $c_p/c^* = 1.5$. The fluid–fluid phase separation is clearly observed in the DIC images, see Fig. 3 and in the confocal microscopy image, see Supplementary Information.

The phase behaviour of hard sphere–polymer mixtures is compared to that of the microgel–polymer mixtures in Fig. 2. It has been observed in the literature, that non-absorbing polymer can cause microgel particles to deswell [12], however, this was not observed during this experiment (see Supplementary Information).

There are a number of differences between the phase diagram of FP and MP mixtures, the most noticeable being the presence of a cluster phase in the MP mixtures and the significantly higher critical polymer concentration needed to induce a phase separation, $\phi^\dagger$, values for the MP mixtures than the FP mixtures, see Fig. 2. For MP0.10 mixtures, twice as much polymer is needed to reach a phase boundary than for FP0.13 mixtures. Furthermore, the fluid–solid phase boundary for the FP mixtures agrees well with theoretical predictions from the literature whereas for the MP mixtures it does not.

Microgel–polymer (MP) mixtures aggregate to form open clusters at $c_p/c^* = 1.5$, for MP0.10, and 0.9 for MP0.20. In MP0.10 the polymer samples are not made with a high enough polymer concentration to form a gel, whereas for MP0.20, samples form a weak gel when $c_p/c^* = 1.9$, see Fig. 2b. The minimum critical polymer concentration needed to induce a phase separation, $\phi^\dagger$, for MP mixtures is significantly higher than the theoretical curve shown in Fig. 2b. The presence of the cluster phase, at $c_p/c^* = 0.9$ can clearly be seen in DIC images of MP0.20 mixtures, see Fig. 3.

The strength of the gels formed can be determined from rheology. In a flow curve, a sample that has formed a gel will be shear thinning, where the viscosity decreases with shear rate. Newtonian flow in a sample, where the viscosity is independent of the shear rate does not indicate the presence of a network [19,20]. All the MP mixtures made show Newtonian behaviour, even at the highest polymer concentrations. Fig. 4a shows the flow curves for MP0.20, and similar data were obtained for MP0.10 mixtures.

A frequency sweep can be used to calculate the elastic (G') and viscous (G'') moduli of a sample. If $G' > G''$ then the sample is elastic and a network has formed, if $G' < G''$ then the sample is viscous and there is no network formed. The formation of a network can also be shown by a jump in the values of the moduli with increasing polymer concentration [21].

The moduli of MP0.20 mixtures as a function of polymer concentration is shown in Fig. 4c where the moduli have been taken at a frequency of 0.5 Hz. At all polymer concentrations, the moduli of these mixtures are very low and only G'' at the highest concentration is above

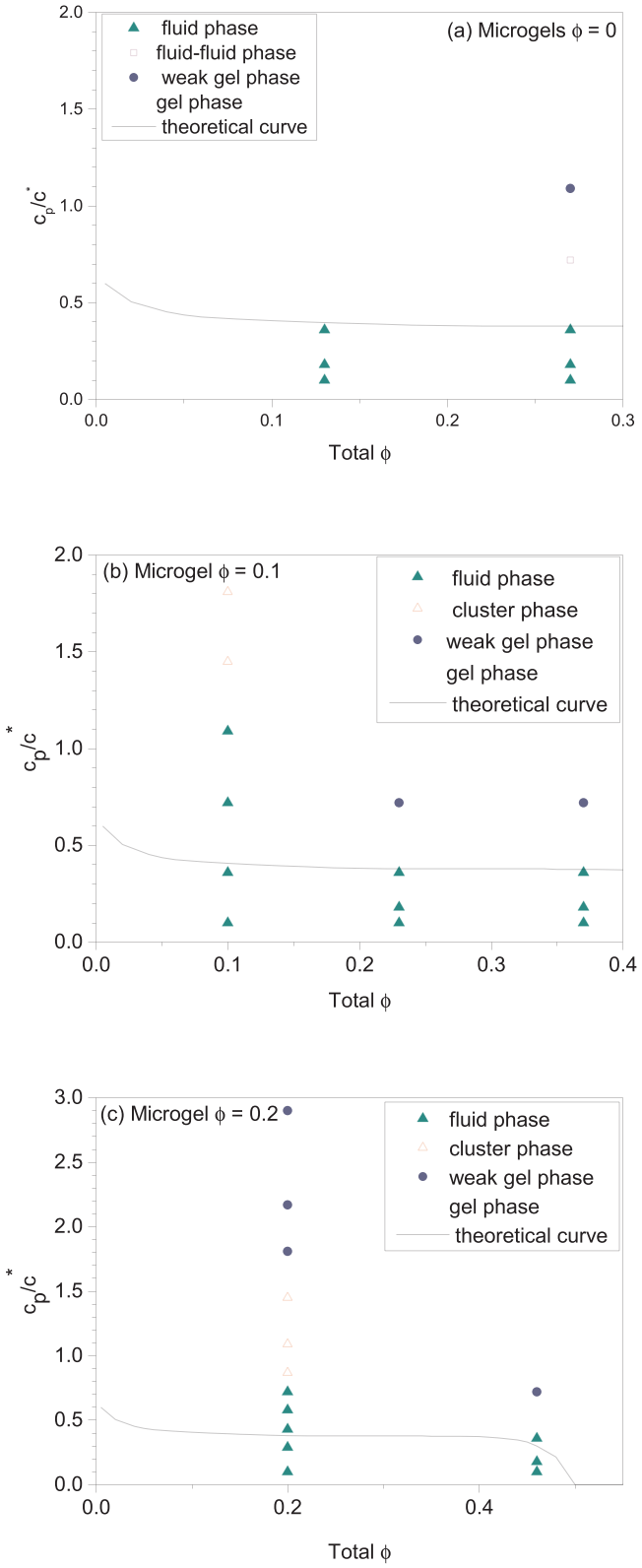

Fig. 5. Phase diagram of microgel–fluorescent poly(styrene)–polymer mixtures. (a) Microgel volume fraction = 0, (b) microgel volume fraction = 0.1 and (c) microgel volume fraction = 0.2. Green filled triangles = stable fluid, red open triangles = clusters, blue filled circles = weak gel, purple open squares = fluid–fluid phase and black open circles = gel. The solid line shows the theoretical curve from Ref. [18] where q_r = 0.34. (For interpretation of the references to color in this figure legend, the reader is referred to the web version of the article.)

0.5 Pa. Furthermore, there is no major increase in the moduli with increasing polymer concentration. Even though the elastic modulus is often above the viscous modulus, these low values indicate that there is no network in the sample. Similar data were obtained for MP0.10 mixtures. Oscillations of samples at such low values provide noisy data and this could explain why G' is often greater than G''.

Both the flow curves and frequency sweeps provide evidence that the MP mixtures do not form gels at any polymer concentration studied. Therefore, any sample that appears to be forming a network in the DIC microscopy and height profiles has been described as a weak gel in Fig. 2a.

The rheology for FP mixtures is also significantly different to MP mixtures. All FP mixtures (apart from the lowest polymer concentrations) are shear thinning and have higher viscosities than the MP mixtures, see Fig. 4b. Furthermore, the elastic and viscous moduli for FP mixtures are higher than for MP mixtures, indicating that the networks formed in FP mixtures are stronger, see Fig. 4c. There is very little difference between the elastic and viscous moduli for the three FP mixtures with the highest c_p/c^* and consequently it is difficult to determine when the samples become gelled. Nonetheless, the phase diagram has been constructed by considering the DIC images, height profiles and rheology together and it is concluded that only the last two samples have gelled, with only the last sample forming a strong gel.

3.2. Ternary mixtures

Three different ternary mixtures were made: MFP0.23, MFP0.37 and MFP0.46, see Table 2. The phase diagrams of these ternary mixtures are shown in Fig. 5 and are compared to a theoretical curve from Ref. [18] where q_r = 0.34, shown by the solid line in Fig. 5 [18].

The ternary mixtures all form weak gels when c_p/c^* = 0.7 and gels when c_p/c^* = 0.9. MFP0.46 has the highest total particle volume fraction and thus it is expected that $\phi^\dagger$ for MFP0.46 would be lower than other MFP mixtures, however, a stable fluid is still present for this sample above the theoretical line shown in Fig. 5c. One possible explanation for this is that the microgel particles are reducing the strength of the depletion interaction and are hence affecting the phase behaviour. The DIC microscopy images show that a space filling network is formed for all MFP mixtures when c_p/c^* = 0.7, see Fig. 3.

There is some evidence that the addition of soft particles affects the phase behaviour of ternary microgel–colloid–polymer mixtures. To further examine the effect of these soft particles on the networks formed during the depletion induced phase separation, the rheology of the mixtures was examined.

Data for gel samples at c_p/c^* = 1.1 are shown in Fig. 6. All samples are shear thinning; whilst the viscosity increases on adding microgel particles, there is a small decrease of the elastic and viscous moduli. This is discussed in detail below. For comparison, data are also shown for fluid samples at c_p/c^* = 0.4. The elastic and viscous moduli decrease with increasing microgel volume fraction. The flow curves (panel b) however show that these samples are still near-Newtonian fluids, and the onset of phase separation or gel formation around c_p/c^* = 0.7 is also in agreement with macroscopic settling behaviour (see Supplementary Information). The effect of replacing microgel particles with hard spheres in binary colloid–polymer mixtures, and adding hard sphere particles to microgel–polymer mixtures was also considered (see Supplementary Information).

3.3. Confocal microscopy

From the DIC microscopy images it is clear to see that MFP mixtures form a space-filling network when c_p/c^* = 0.7 or higher. CLSM can be used to determine if the two types of particles flocculate to form a homogeneous network or two separate, inter-penetrating networks [22]. Microgel

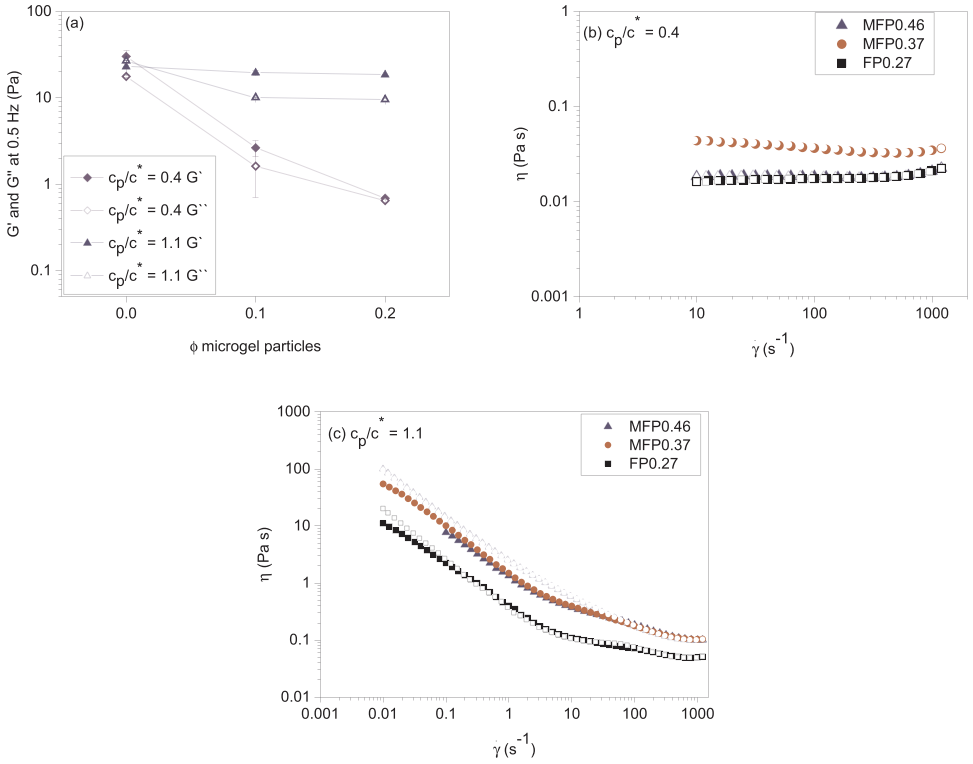

Fig. 6. (a) The elastic (G') and viscous moduli (G'') at 0.5 Hz for FP0.27 with increasing microgel volume fraction, for polymer concentrations $c_p/c^* = 0.4$ (purple diamonds) and 1.1 (blue triangles). Lines are to guide the eye. (b) Viscosity, η as a function of shear rate, $\dot{\gamma}$, for FP0.27 (black squares), MFP0.37 (red circles) and MFP0.46 (blue triangles) with $c_p/c^* = 0.4$. (c) Viscosity, η, as a function of shear rate, $\dot{\gamma}$, for FP0.27 (black squares), MFP0.37 (red circles) and MFP0.46 (blue triangles) with $c_p/c^* = 1.1$. Filled symbols are for increasing shear rate and open symbols are for decreasing shear rate. (For interpretation of the references to color in this figure legend, the reader is referred to the web version of the article.)

particles were dyed with Sudan 2 according to Section 2.2.1 and an MFP0.37 mixture with $c_p/c^* = 0.7$ was made and examined. The two particles both form the same homogeneous network and, although there are a few regions that could be described as either microgel or hard sphere rich, there is no evidence of two separate inter-penetrating networks, see Fig. 7.

4. Discussion

4.1. Depletion interactions

The depletion attraction between two colloidal particles immersed in a polymer solution is proportional to the overlap volume of the depletion zones surrounding the two spheres (V_{ov}), which in turn depends on the centre to centre particle separation r_i, the particle radius r and the thickness of the depletion layer β [7]. The effective depletion radius r_d then follows as:

$$r_d = r + \beta \tag{2}$$

and

$$V_{ov} = \frac{4\pi}{3} r_d^3 \left[1 - \frac{3}{4}\frac{r_i}{r_d} + \frac{1}{16}\left(\frac{r_i}{r_d}\right)^3 \right]. \tag{3}$$

The maximum extent of overlap ($d_{ov(max)}$) (resulting in the maximum overlap volume) for any two particles is given by $2(r_d - r)$. This is equal to sum of the depletion layer thicknesses for the two particles, see Fig. 8. Therefore, particles with a large depletion layer thickness β will have a large maximum extent of overlap and hence a strong depletion interaction. For the soft microgel particles, β is smaller than for the hard particles due to the penetration of the non-adsorbing polymer into the soft microgel particles [3,4,7]. Therefore, $d_{ov(max)}$ for two soft particles is smaller than for two hard particles and $d_{ov(max)}$ for a system of one hard particle and one soft particle is in-between the two. Consequently, the depletion contact is strongest between two hard particles, weakest between two soft particles and in between for a hard-soft contact.

4.2. Binary mixtures

In all mixtures, increasing the overall particle volume fraction decreases $\phi^\dagger$ in agreement with the literature [3]. $\phi^\dagger$ for MP mixtures is significantly higher than for FP mixtures, particularly for MP0.10 where twice as much polymer is needed to induce aggregation than for FP0.13. The main reason for this difference in $\phi^\dagger$ is the weakened depletion interaction in MP mixtures due to penetration of the polymer into the particles. Highly cross-linked poly(styrene) particles are harder than microgels and thus there is less penetration and the depletion interaction is stronger [3,4,23].

Furthermore, the microgel particles are made of only poly(styrene) without any additional polymer stabilising the particles. The mixing between the poly(styrene) particles and the non-adsorbing poly (styrene) is favourable, which encourages penetration and weakens the depletion interaction further [3,5]. The highly cross-linked particles are stabilised with a comb copolymer which is not made of poly(styrene). This stabilising polymer has unfavourable mixing with the non-adsorbing poly(styrene) which reduces the likelyhood of polymer penetrating into the harder particles.

Another major difference between the MP and FP mixtures is the formation of a stable cluster phase in the MP mixtures. Such phases exist when there is a competition between depletion attraction and long range repulsions, limiting the size of the aggregates. Typically the long ranged repulsion results from electrostatic interactions on the colloidal particles where double layer interactions act as a soft repulsive barrier between the particles [7]. The electrostatic interactions in charged colloid–polymer mixtures also result in a higher polymer concentration needed to induce a phase separation.

The cluster size depends on the relative ratios of the repulsive and attractive interactions and their properties are time independent [24]. Stradner et al. demonstrate the universality of these clusters using two different model systems: protein solutions and colloid–polymer mixtures using small angle neutron scattering and confocal microscopy [25]. Zhou et al. studied the depletion induced phase separation of charged silica particles on the addition of non-adsorbing poly(styrene) and their experimental data was successfully modelled using theoretical

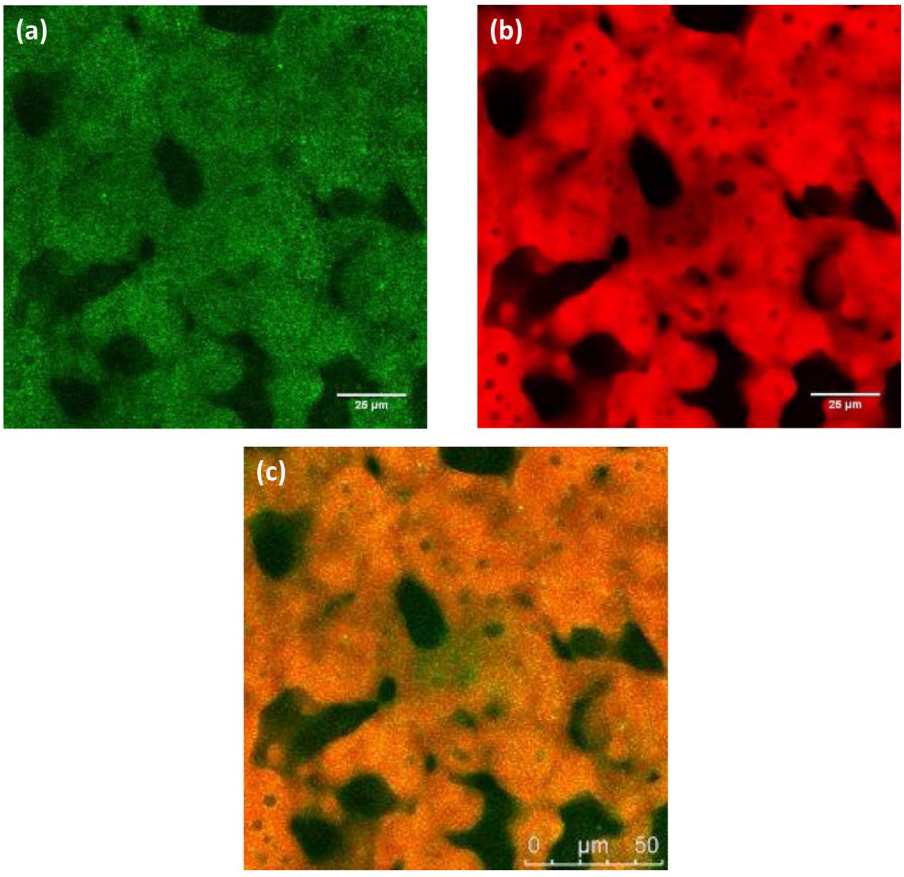

Fig. 7. Confocal laser scanning microscopy images of an MFP0.37 mixture with $c_p/c^* = 0.7$. The microgel particles are dyed with Sudan 2. (a) Fluorescence from the microgel particles dyed with Sudan 2, (b) fluorescence from the highly cross-linked particles dyed with rhodamine B and (c) the fluorescence from both the microgel particles and the highly cross-linked particles.

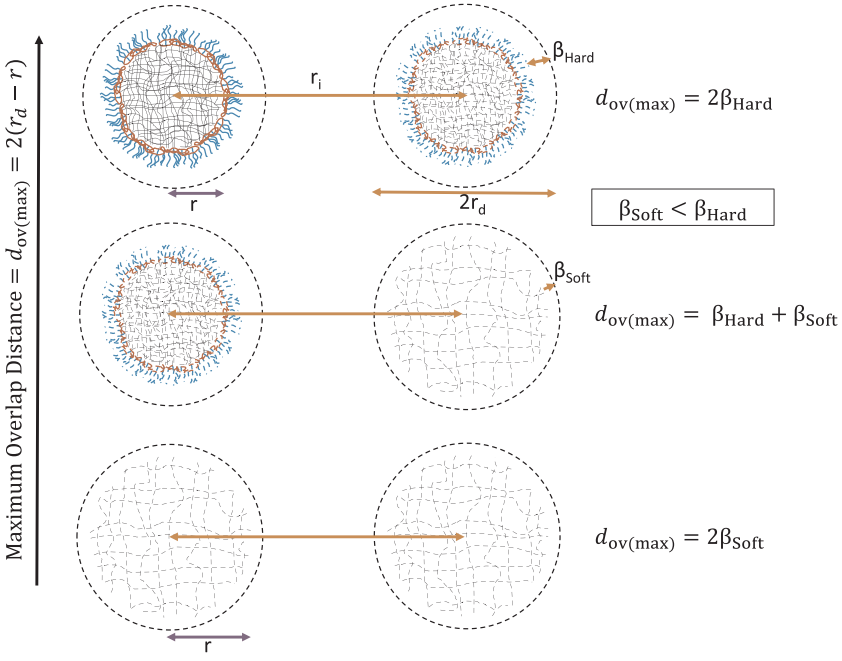

Fig. 8. The maximum overlap distance between two hard spheres (top), one hard sphere and one soft microgel particle (middle) and two soft microgel particles (bottom).

predictions by Gögelein and Tuinier [27]. They demonstrated that adding salt screens the electrostatic interactions and enables the attractive interactions to dominate, resulting in more straightforward phase behaviour, where no clusters were present [26]. Charges on the microgel particles could provide an explanation for the stable cluster phase seen in the microgel–polymer mixtures.

Sedgwick et al. looked at the effect of density matching on the phase separation of charged and charge screened colloid–polymer mixtures. For charge screened, density matched mixtures they also saw clusters above a critical polymer concentration. These clusters were caged by their nearest neighbours which suspended long range motion and prevented large aggregates from forming. Furthermore, the clusters did not sediment under gravity. They described the formation of these mixtures using mode coupling and cluster mode coupling theories [28]. Microgel

particles are predominately made of solvent and hence are close to a density matched system. Therefore, even (small) clusters of microgel particles will not sediment under gravity and a stable cluster phase is possible.

4.3. Ternary mixtures

In the ternary mixtures, the soft microgel particles behave differently to the highly cross-linked poly(styrene) hard spheres. The relationship between the microgel volume fraction and network strength is not straightforward and depends on the polymer concentration and subsequent phase of the mixtures.

Adding microgels to a hard sphere–polymer mixture does not appear to affect the interactions between the particles significantly, particularly at a high polymer concentration, see Fig. 6. When soft particles are added to a hard sphere–polymer mixture, two opposing interactions occur which counteract each other. The overall particle volume fraction of the mixture increases which should increase the network strength, however, the soft microgel particles weaken the systems and therefore the overall particle strengths do not significantly change.

This counterbalance between two opposing processes helps to explain why all three ternary mixtures have the same $\phi^{\dagger}$. For MFP0.23 the overall particle volume fraction is the lowest, however the microgel volume fraction is also the lowest, hence the depletion interaction is similar to MFP0.46 which has a higher total particle volume fraction but also a higher microgel volume fraction.

The polymer concentration also influences the strength of the depletion interaction and the effect of the microgel particles. Below $\phi^{\dagger}$, where the samples form stable fluids, the addition of microgel particles reduces the elastic and viscous moduli and does not greatly affect the viscosity. Above $\phi^{\dagger}$, however, the elastic and viscous moduli are independent of the microgel volume fraction; the viscosity increases significantly with increasing the microgel volume fraction, see Fig. 6. In a stable fluid, the microgels should be fully swollen and hence the softness of the mixtures dominates the interparticle attractions. Therefore, even though the overall volume fraction is increased, the interactions between the particles are weak.

In a gel the interactions between the particles are already significantly larger than in a stable fluid. Therefore, the increase in the overall particle volume fraction dominates the interparticle strengths and hence the depletion interaction strength increases. Over this threshold, the softness of the particles has less impact on the overall interaction strength.

High volume fractions typically result in aggregation and high viscosities, particularly when a non-adsorbing depletant is added. It is shown here that, by using microgel particles, it is possible to reach a high volume fraction without inducing aggregation and producing solutions with high viscosities. Such behaviour has applications in formulating concentrated suspensions, where low viscosities are required.

5. Conclusion

The phase behaviour of ternary microgel–colloid–polymer mixtures has been studied and compared to binary mixtures of each particle with non-adsorbing polymer. DIC microscopy, height profiles, rheology and confocal microscopy are used to analyse the mixtures and a phase diagram for each system is constructed. The combination of different techniques is necessary to determine the phase behaviour studied here.

MP mixtures behave very different to FP or MFP mixtures and they have a significantly higher $\phi^{\dagger}$. The depletion interaction of these soft particles is weakened due to penetration of the non-adsorbing polymer into the particle. Furthermore, the near density matched particles are able to display a stable cluster phase as the small aggregates do not settle under gravity.

The MFP and FP mixtures, however, have very similar phase diagrams which agree well with a free volume perturbation theory for a colloid–polymer mixture with a similar size ratio. The addition of soft microgels to the hard sphere–polymer mixtures does not greatly affect $\phi^{\dagger}$ due to the counteracting forces that occur when the microgels are added. The addition of soft particles to the system weakens the interparticle interactions. The increase in the total volume fraction, however, strengthens the particle interactions. Consequently the overall phase behaviour remains largely unchanged.

Rheological studies have been used to probe the difference in the particle interaction strengths further. Adding microgels to a hard sphere–polymer mixture does not significantly affect the particle interaction strength, particularly at high polymer concentrations. This is due to the two counteracting effects of the microgel particles. At low polymer concentrations, however, the effect of the particle softness appears to dominate the interaction strength and hence adding microgels to a hard sphere–polymer mixture actually decreases the interparticle interactions.

Confocal microscopy was used on one sample with a fixed particle volume fraction and it was concluded that a homogeneous network of both hard and soft particles is formed. This is consistent with the depletion interactions between soft and hard particles being stronger than those between two soft particles.

Financial funding and support

Funding for this work was provided by Bayer CropScience AG and the EPSRC (DTA ref EP/K502996/1).

Conflict of interest

The author declares that there are no conflicts of interest.

Acknowledgements

The authors acknowledge C. P. Royall, C. Ferreiro Cordova and I. Rios De Anda for training and access to the confocal microscope and E. Alred for training on the rheometer.

Appendix A. Supplementary data

Supplementary data associated with this article can be found, in the online version, at http://dx.doi.org/10.1016/j.colsurfa.2017.07.022. Rheology data are available at the University of Bristol data repository, data.bris, at https://doi.org/10.5523/bris.97ywxg6qnmhx23qb2wcwyb3vf.

References

[1] C.P. Royall, W.C.K. Poon, E.R. Weeks, Soft Matter 9 (2013) 17–27.
[2] W.C.K. Poon, J. Phys.: Condens. Matter 14 (2002) 859–880.
[3] A. Milling, B. Vincent, S. Emmett, A. Jones, Colloid Surf. 57 (1991) 185–195.
[4] B. Vincent, J. Clarke, K.G. Barnett, Colloid Surf. 17 (1986) 51–65.
[5] A. Jones, B. Vincent, Colloid Surf. 42 (1989) 113–138.
[6] C. Sieglaff, J. Polym. Sci. 41 (1959) 319–326.
[7] H.N.W. Lekkerkerker, R. Tuinier, Colloids and the Depletion Interaction, Springer, 2011.
[8] S. Burger, E. Bartsch, Colloid Surf. 442 (2014) 6–15.
[9] A. Kozina, P. Diaz-Leyva, C. Friedrich, E. Bartsch, Soft Matter 8 (2012) 1033–1046.
[10] E. Bartsch, T. Eckert, C. Pies, H. Sillescu, J. Non-Cryst. Solids 307–310 (2002) 802–811.
[11] M. Wiemann, N. Willenbacher, E. Bartsch, Colloid Surf. A 413 (2012) 78–83.
[12] B.R. Saunders, B. Vincent, Colloid Polym. Sci. 275 (1997) 9–17.
[13] J. Clarke, B. Vincent, J. Chem. Soc. Faraday Trans. 77 (1981) 1831–1843.
[14] M. Schmidt, A.R. Denton, Phys. Rev. E: Stat. Nonlinear Soft Matter Phys. 65 (2002) 021508.

[15] A. Esztermann, H. Reich, M. Schmidt, Phys. Rev. E 73 (2006) 011409.
[16] Y. Hennequin, M. Pollard, J.S. van Duijneveldt, J. Chem. Phys. 120 (2004) 1097–1104.
[17] M.A. Faers, P.F. Luckham, Langmuir 13 (1997) 2922–2931.
[18] P.G. Bolhuis, A.A. Louis, J.-P. Hansen, Phys. Rev. Lett. 89 (2002) 128302.
[19] W.B. Russel, The Phase Behavior and Dynamics of Colloidal Dispersions, Lecture Notes Debye Professor 200-2001, (2005).
[20] P. Patel, W. Russel, J. Colloid Interface Sci. 131 (1989) 201–210.
[21] M.A. Faers, G.R. Kneebone, Pest. Sci. 55 (1999) 312–325.
[22] L. Di Michele, F. Varrato, J. Kotar, S. Nathan, G. Foffi, E. Eiser, Nat. Commun. 4 (2013) 1–7.
[23] N. Cawdery, A. Milling, B. Vincent, Colloid Surf. A 86 (1994) 239–249.
[24] R. Sanchez, P. Bartlett, J. Phys.: Condens. Matter 17 (2005) S3551.
[25] A. Stradner, H. Sedgwick, F. Cardinaux, W.C.K. Poon, S.U. Egelhaaf, P. Schurtenberge, Nature 432 (2004) 492–495.
[26] J. Zhou, J.S. van Duijneveldt, B. Vincent, Langmuir 26 (2010) 9397–9402.
[27] C. Gögelein, R. Tuinier, Eur. Phys. J. E 27 (2008) 171–184.
[28] H. Sedgwick, S.U. Egelhaaf, W.C.K. Poon, J. Phys.: Condens. Matter 16 (2004) S4913.